Direct measurement of Surface interaction between microcapsule for DDS and artificial mucin layers by using colloid probe AFM

Hidehiro Kamiya, Motoyasu Yoshimura, Tadashi Tsuchiya, Motoyuki Iijima

Tokyo University of Agriculture and Technology, Koganei, Tokyo 184-8588, Japan

Hideki Ichikawa, Yoshinobu Fukumori,

Faculty of Pharmaceutical Sciences and Co-operative Research Center of Life Sciences,

Yoshifumi Takeuchi

Gifu Pharmaceutical University, Japan

A novel thermo- and pH-sensitive nanogel particle, which is a core-shell structured particle with a poly(*N*-isopropylacrylamide) (p(NIPAAm)) hydrogel core and a poly(ethylene glycol) monomethacrylate grafted poly(methacrylic acid) (p(MMA-g-EG)) shell, is of interest as a vehicle for the controlled release of peptide drugs. The interactions between such nanogel particles and artificial mucin layers during both approach and separation were successfully measured by using colloid probe atomic force microscopy (AFM) under various conditions. While the magnitudes of the compression forces and scan velocities did not affect the interactions during the approach process, the adhesive force during the separation process increased with these parameters. The pH values significantly influenced the interactions between the nanogel particles and a mucin layer. A large steric repulsive force and a long-range adhesive force were measured at neutral pH due to the swollen p(MMA-g-EG) shell. On the other hand, at low pH values, the steric repulsive force disappeared and a short-range adhesive force was detected, which resulted from the collapse of the shell layer. The nanogel particles possessed a pH response that was sufficient to protect the incorporated peptide drug under the harsh acidic conditions in the stomach and to effectively adhere to the mucin layer of the small intestine, where the pH is neutral. The relationships between the nanogel particle–mucin layer interactions, pH conditions, and other parameters were systemically investigated and discussed. Furthermore, chitosan-coated liposomes have been designed for same purposes. Carbon nano-tube (CNT) attached probe was immersed in PEI solution (3mg/ml) over night and then adsorbed mucin layer on CNT probe. Micro adhesion behavior of chitosan-coated liposomes was quantitatively assessed by using CNT probe with coated mucin layer.

Design and characterization of liposomal nano-particles for effective drug delivery

Hirofumi Takeuchi
Laboratory of Pharmaceutical Engineering, Department of Drug Delivery Technology and Science, Gifu Pharmaceutical University,
5-6-1 Mitahora-Higashi, Gifu 502-8585, Japan.

Colloidal drug carriers, such as liposomes, lipid emulsions, and polymeric nanoparticles have great potential to provide effective drug delivery. A variety of investigations have been carried out for designing an optimal particulate system for drug delivery in topical administration as well as in systemic administration.

Liposome is one of most promising drug carriers, because its particle size and surface charge are easily controlled. We have also demonstrated feasibility of surface design of liposomes by coating its surface with functional polymers. The resultant polymer-coated liposomes showed higher stability in storage, prolonged blood circulation after intravenous injection, and mucoadhesive property.

We have demonstrated feasibility of polymer coating of liposomes. For example, negatively charged liposomes were coated with various hydrophilic polymers—such as polyvinyl alcohol (PVA); a modified PVA, which bears a long alkyl chain at the end of the molecule (PVA-R); poly(acrylic acid)-bearing cholesterols (PAA-Chol); and chitosan (CS)—by simply mixing the liposomal suspension with the polymer solution . We have observed their retentive and penetrative properties on mucus layer of intestine after their oral administration. These behaviors lead to enhancement in absorption of peptide drugs such as insulin in rats.

We have also revealed that the surface modification of liposomes with the polymers enabled the control of liposome behavior in the lung as well as in the bloodstream and gastrointestinal tract. The results suggest that pulmonary administration of drug with polymer-coated liposomes can provide a high level of efficiency by controlling its behavior.

The posterior segment-related diseases including age-related macular degeneration (ARMD), diabetic macular edema (DME) and endophthalmitis tend to cause serious symptoms such as vision impairment and blindness. The drugs for these diseases are generally administered via invasive methods such as intravitreal injections and sub-tenon injections, because non-invasive application such as eye drops are not effective in delivering drugs into the posterior segments. We have tried to demonstrate the usefulness of liposomal systems for delivering drug to the posterior segments of the eye by designing the liposomal formulation containing a fluorescence marker. The time course of fluorescence intensity at retina calculated with ImageJ software after administration of several types of liposomal formulation confirmed these tendencies. This observation strongly suggested that the nano-liposomes can effectively deliver the drug to the posterior part of the eye.

Pharmaceutically engineered gadolinium-loaded nanoparticles for MR-imaging and neutron-capture therapy of cancer

Hideki Ichikawa
Faculty of Pharmaceutical Sciences and Cooperative Research Center of Life Sciences,
Kobe Gakuin University, Kobe, Japan

Gadolinium neutron-capture therapy (Gd-NCT) is a cancer therapy that utilizes γ-rays and electrons emitted as a result of ^{157}Gd (n, γ) ^{158}Gd reaction in vivo. Several researchers have evidenced the potential of Gd-NCT in recent years by using gadolinium-based MRI contrast agents such as Magnevist® (dimeglumine gadopentetate) and Gadovist® (macrocyclic Gd complex). However, in vivo performance in Gd-NCT has not been sufficiently established yet, because these commercially available Gd agents are, even if intratumorally (i.t.) injected with an extremely high dose, eliminated rapidly from tumor tissues due to their non-affinity to tumor, resulting in poor accumulation and retention in tumor.

In this context, we have developed novel gadopentetic acid (Gd-DTPA)-loaded chitosan nanoparticles (Gd-nanoCP) as an injectable device capable of maintaining a sufficient Gd concentration in the tumor during the treatment. The primary idea to achieve the improved accumulation of Gd in tumor using Gd-nanoCPs relies on the use of chitosan with bioadhesive (cationic), biocompatible (nontoxic) and biodegradable (bioerodible) natures in the nanoparticulate form. The Gd-nanoCPs were prepared by a newly developed emulsion coalescence technique. The particle size, zeta potential and Gd content can be controlled in the range of 150-750 nm, 20-30 mV and 7-23 wt%, respectively, by altering Mw and deacetylation degree of chitosan and its concentration in the solution.

The in vitro cellular accumulation behaviors of Gd-nanoCPs were evaluated in three cultured cell lines including L929 fibroblast cells, B16F10 melanoma cells and SCC-VII squamous cell carcinoma. These cells were incubated with sterilized Gd-nanoCPs (40 ppm as the feed Gd concentration) for 12h at 37°C and subsequently washed with PBS to remove free Gd and Gd-nanoCPs. Magnevist® was used as a control. The amounts of Gd per 10^6cells detected in the washed cells were approximately 100-200 times higher in comparison to Magnevist®, indicating that Gd-nanoCPs have a high affinity to the cells. Furthermore, the endocytic cellular uptake of Gd-nanoCPs was confirmed by transmission electron microscopic observation and comparative studies between at 4°C and 37°C.

The Gd-NCT trial using Gd-nanoCPs was carried out in vivo. Gd-nanoCPs were i.t. injected twice to mice bearing subcutaneous B16F10 melanoma. Eight hours after the second injection, the thermal neutron irradiation was performed at the tumor site, with the fluence of 6.32×10^{12} neutrons/cm^2. The tumor growth in the Gd-nanoCPs administered mice was significantly suppressed by the neutron irradiation while no effect was observed in the Magnevist® administered mice. Obviously, the significant tumor-growth suppression was ascribed from the long-term retention of Gd in tumor tissue. It is noteworthy that the significant Gd-NCT effect was achieved even in the radio-resistant melanoma where a long interval existed between Gd-nanoCP injection and neutron irradiation with a smaller gadolinium dose.

In conclusion, the present study demonstrated that the pharmaceutically engineered gadolinium-loaded chitosan nanoparticles would be an effective device to improve the efficacy of Gd-NCT. Another prospect of the Gd-nanoCPs containing Gd-DTPA is the capability of medical tool for the non-invasive diagnosis of tumorigenic diseases. Our preliminary experiments revealed that the Gd-nanoCPs can be visualized by the MRI system in the cultured human sarcoma cells. In this talk, the performance of the Gd-nanoCPs as a MRI contrast agent will be also discussed briefly.

References:

1. H. Tokumitsu, H. Ichikawa, Y. Fukumori, *Pharm. Res.*, **16**, 1830-1835 (1999).
2. H. Tokumitsu, J. Hiratsuka, Y. Sakurai, T. Kobayashi, H. Ichikawa, Y. Fukumori, *Cancer Lett.*, **150**, 177-182 (2000).
3. F. Shikata, H. Tokumitsu, H. Ichikawa, Y. Fukumori, *Eur. J. Pharm. Biopharm.*, **53**, 39-49 (2000).
4. Y. Fukumori, H. Ichikawa, *Drug Delivery Systems*, **17**, 355-364 (2002).
5. P. Sharma, S.C. Brown, G. Walter, S. Santra, E. Scott, H. Ichikawa, Y. Fukumori, B.M. Moudgil, *Adv. Powder Tech.*, **16**, 663-698 (2007).
6. T. Fujimoto, H. Ichikawa, et al., *Appl. Rad. Ther.*, **67**, S355-S358 (2009).

In vivo imaging of tumor malignancy with near-infrared fluorescence probes targeting HIF-active cells

Shinae Kizaka-Kondoh[1, 2], Takahiro Kuchimaru[1, 2], Tetsuya Kadonosono [1, 2] and Masahiro Hiraoka[1,]

[1] Department of Radiation Oncology and Image-applied Therapy, [2]Innovative Techno-Hub for Integrated Medical Bio-imaging, Kyoto University Graduate School of Medicine, Kyoto, Japan

In solid tumors, the distribution of oxygen pressure is not homogenous because of the uncontrolled tumor growth and immature blood vessels during angiogenesis, which generate a hypoxic microenvironment. Tumor hypoxia causes resistance to radiotherapy and chemotherapy, and malignant progression Hypoxia-inducible factor-1 (HIF-1) is a master transcriptional regulator for adaptation to hypoxia. Many of the genes induced by HIF are critically involved in aspects of cancer biology, including immortalization, maintenance of stem cell pools, cellular differentiation, genetic instability, vascularization, metabolic reprogramming, autocrine growth factor signaling, invasion/metastasis and resistance to treatment. Therefore, early detection of HIF-active regions is important for initiating timely and appropriate treatments for malignant cancers. We have been developing fusion protein probes specific to HIF-1-active microenvironment for imaging and targeting malignant tumors. We recently constructed a fusion protein POH, which consisted of Protein Transduction Domain (PTD), Oxygen-dependent Degradation Domain (ODD) and HaloTag. The PTD was a membrane-permeable peptide, which efficiently delivered fusion proteins into cells. The ODD was responsible for the oxygen-dependent regulation of the probe, which stabilizes in a hypoxic environment and degrades immediately under normoxic conditions. In addition, HaloTag was used to covalently conjugate with its specific ligand labeled with near-infrared fluorescence (NIRF) dye. To visualize the targets *in vivo*, we used bioluminescence imaging of tumor cells, which stably retained a HIF-1-dependent luciferase reporter gene. POH-NIRF probes successfully imaged HIF-1-active regions in subcutaneously implanted human xenograft tumors and orthotopic pancreatic cancers with IVIS-SPECTRUM 9 to 24 hrs after POH-NIRF injection. Furthermore, immunohistochemical analysis of tumor sections from the mice 6h after POH-NIRF injection revealed the regions imaged with POH-NIFR was overlapped with HIF-1α-positive regions, while the intracellular localization of POH-NIRF is in cytoplasm. Overall results demonstrated that POH-NIRF is a specific probe for HIF-1-active/hypoxic cells and suggested that a PTD-ODD probe would become a unique imaging probe for malignancy.

Ⅴ．研究成果の刊行に関する業績一覧

発表者名	論文タイトル名	発表雑誌名	巻号	ページ	出版年
Fujioka K, Manabe N, Nomura M, Watanabe M, Takeyama H, Hoshino A, Hanada S, Yamamoto K., Manome Y.	Detection of thyroid carcinoma antigen with Quantum dots and monoclonal IgM antibody (JT-95) systems.	*J. Nanomater*			In press
Yamamoto S, Manabe N, Yamamoto K.	High-Definition Slit Lamp Video Camera System	*Ophthalmic Surgery, Lasers & Imaging*	Vol. 41, No.1		2010
Shiohara A, Hanada S, Prabakar S, Fujioka K, Lim T, Yamamoto K, Northcote P, Tilley RD.	Chemical Reactions On Surface Molecules Attached to Silicon Quantum Dots.	*J Am Chem Soc.*	Jan 13;132(1)	248-253	2010
Fujioka K, Arakawa E, Kita J, Aoyama Y, Okuda T, Manome Y, Yamamoto. K.	Combination of Real-Value Smell and Metaphor Expression Aids Yeast Detection.	*PLoS ONE*	4 (11)	e7939	2009
Shiohara. A, Hanada. S, Prabakar. S, Fujioka. K, Lim. T, Yamamoto. K, Northcote. P, and Tilley. RD	Size Controlled Synthesis of Germanium Nanocrystals with Hydride Reducing Agents and their Biological Applications	*Chemistry of Materials*			In press

Sudoh K, Hirakuri K, Fujioka K, Manabe N, Yamamoto K	Nanocrystalline diamond particles dispersed by solutions	*Trans Mater Res Soc Jpn .*	34(2)	313-316	2009
Fujioka K, Futamura Y, Shiohara T, Hoshino A, Kanaya F, Manome Y, Yamamoto K	Amino Acid Synthesis in Supercritical Carbon Dioxide with Water System.	*International Journal of Molecular Sciences*			
Hoshino A, Hanada S, Manabe N, Nakayama T, Yamamoto K.	Immune Response Induced by Fluorescent Nanocrystal Quantum Dots *in vitro* and *in vivo*.	*IEEE Transactions on NanoBioscience*	Mar;8(1)	51-57 *Epub ahead of print, Mar 16, 2009.*	2009
Dohi T, Borodovsky A, Wu P, Shearstone JR, Kawashima R, Runkel L, Rajman L, Dong X, Scott ML, Michaelson JS, Jakubowski A, Burkly LC.	TWEAK/Fn14 Pathway: a nonredundant role in intestinal damage in mice through a TWEAK/intestinal epithelial cell axis.	Gastroenterology	136	912-923	2009
Michael S. Patrick, Hiroyo Oda, Kunihiro Hayakawa, Yoshinori Sato, Koji Eshima, Teruo Kirikae, Shun-ichiro Iemjura, Mutsunori Shirai, Takaya	Gasp, a Grb2 associating protein, is critical for positive selection of thymocytes	***Proc. Natl. Acad. Sci. USA***	106	16345-16350	2009

Abe, Tohru Natsume, Takehiko Sasazuki and Harumi Suzuki					
Yoshinori Sato, Hiroyo Oda, Michael S. Patrick, Yukari Baba, Ahmed A. Rus'd, Yoshinao Azuma, Takaya Abe, Mutsunori Shirai and Harumi Suzuki	Rac GTPases are involved in development, survivalannd homeostatic proliferation of T cells	***Immunol. Let.***	124	27-34	2009
Dai Chida; Tsuyoshi Sato; Yoshinori Sato; Mitsumasa Kubo; Tetsuya Yoda; Harumi Suzuki; Yoichiro Iwakura	Characterization of mice deficient in Melanocortin 2 receptor on a B6/Balbc mix background	***Mol Cell Endocrinol.***	300	32-36	2009
Hiroyo Oda, Manabu Fujimoto, Michael S. Patrick, Dai Chida, Yoshinori Sato, Hiroki Aoki, Yoshinao Azuma, Takaya Abe, Harumi Suzuki and Mutsunori Shirai	RhoH plays critical roles in FceRI-dependent signal transduction of mast cells 33--Kinase	***J. Immunol.***	182	957-962	2009
Kei Takahashi, Toshiaki	Administration of	Modern			In press

Oharaseki, Noriko Nagi-Miura, Naohito Ohno, Akiko Ishida-Okawara, Hitomi Yamada, Yoshiaki Kaneshiro, Shiro Naoe, Kazuo Suzuki.	human immunoglobulin inhibited development of vasculitis in a murine model of vasculitis induced with CAWS, *Candida albicans* water soluble fraction.	Reumatol.			
Masumitsu Hatta, Natsuo Yamamoto, Akiko Miyazato, Kiwamu Nakamura, Ken Inden, Tetsuji Aoyagi, Kazuo Suzuki, Mitsuo Kaku, Kazuyoshi Kawakami.	Early production of tumor necrosis factor-α by Gr-1+CD11b+ mononuclear cells and its role in the host defense to pneumococcal infection in lungs.	FEMS Immunol Med Microbiol			In press
Akihiro Hasegawa, Katsuhiro Hayashi, Hiroyuki Kishimoto, Meng Yang, Soichi Tofukuji, Kazuo Suzuki, Hiroshi Nakajima, Robert Hoffman, Mutsunori Shirai, Toshinori Nakayama.	Color-coded real-time cellular imaging of T lymphocyte accumulation and focus formation in mouse asthma model.	J Allergy Clin Immunol	125	461-8	2010

Miura NN, Komai M, Adachi Y, Osada N, Kameoka Y, Suzuki K, Ohno N.	IL-10 is a negative regulatory factor of CAWS-vasculitis in CBA/J mice as assessed by comparison with Bruton's tyrosine kinase-deficient CBA/N mice.	J Immunol.	183(5)	3417-24	2009
Hirahashi J, Hishikawa K, Kaname S, Tsuboi N, Wang Y, Simon DI, Stavrakis G, Shimosawa T, Xiao L, Nagahama Y, Suzuki K, Fujita T, Mayadas TN.		Circulation.	120(13)	1255-65	2009
Yuka Osaki, Yasuhiro Maehara, Masaki Sato, Akiyoshi Hoshino, Kenji Yamamoto, Tomokazu Nagao, Kazuo Suzuki, Shoji Kawachi.	Analysis of cytokines in broncho-alveolar lavage fluids of patients with ARDS: Increase of IL-6, G-CSF, MCP-1, MIP-1ß.	JJSICM(Journal of Japanese Society of Intensive Care.			2009 In press
Shoji Kawachi, San Thi Luong, Mika Shigematsu, Hiroyuki Furuya, Thuy Thi Bich Phung, Phuc Huu Phan, Hiroyuki Nunoi, Liem	Risk parameters of fulminant acute respiratory distress syndrome followed by avian influenza (H5N1) infection in Vietnamese children.	J. Infectious Dis.	200	510-515.	2009

Thanh Nguyen, Kazuo Suzuki.					
Chiaki Kaga, Shigeyuki Nomura, Mina Okochi, Tomoko Nozu, Tomokazu Nagao, Atsushi Nagai, Toshinori Nakayama, Kazuo Suzuki, Hiroyuki Honda.	Screening of epithelial cell-adhesive peptides from fibronectin loop region and its cell specificity.	J Chem. Engineering Japan	4	298-302.	2009
Tomoko Nozu, Mitsuko Kondo, Kazuo Suzuki, Jun Tamaoki, Atsushi Nagai.	A Comparison of the Clinical Features of ANCA-Positive and ANCA-Negative Idiopathic Pulmonary Fibrosis Patients.	Respiration	77	407-415.	2009
長尾朋和、鈴木和男	ANCA 関連血管炎と Neutrophil Extracellular Traps(NETs、好中球細胞外補足構造)	リウマチ科			In press
Keiko Suzuki and Shoji Yamada	Triacylated lipopeptide, a component of Gram-positive bacteria, induces osteoclastogenesis in the absence of RANKL and resorbs calvarial	Oral Ther Pharmacol,			In press

	bone *in vivo* through Toll-like receptor 2				
Nobuhiro Sakai, Keiko Suzuki, Tomio Morohashi and Shoji Yamada	Na+/Ca2+ exchanger mRNA and orientation of F-actin filaments in cultured osteoblastic cells	Dent Med Res			In press
Kouki Fujioka, Noriyoshi Manabe, Mayumi Nomura, Michiko Watanabe, Hiroshi Takeyama, Akiyoshi Hoshino, Sanshiro Hanada, Kenji Yamamoto, and Yoshinobu Manome	Detection of thyroid carcinoma antigen with Quantum dots and monoclonal IgM antibody (JT-95) systems	*Nanomater*			2010 Accepte d
Takeshita F, Hokaiwado N, Honma K, Banas A, Ochiya T.	Local and systemic delivery of siRNAs for oligonucleotide therapy. Sioud M (eds), siRNA and miRNA Gene Silencing.	Sioud M (eds), siRNA and miRNA Gene Silencing.		83-92	2009
Morita S, Hara A, Kojima I, Horii T, Kimura M, Kitamura T, Ochiya T, Nakanishi K, Matoba R,	Dicer is required for maintaining adult pancreas.	PLoS ONE	4	e4212	2009

Matsubara K, Hatada I.					
Honma K, Takemasa I, Matoba R, Yamamoto Y, Takeshita F, Mori M, Monden M, Matsubara K, Ochiya T.	Screening of potential molecular targets for colorectal cancer therapy.	nt J Gen Med.	2	243-257	2009
Yamamoto Y, Kosaka N, Tanaka M, Koizumi F, Kanai Y, Mizutani T, Murakami Y, Kuroda M, Miyajima A, Kato T, Ochiya T.	MicroRNA-500 as a potential diagnostic marker for hepatocellular carcinoma.	Biomarkers	14	529-538	2009
Harada-Shiba M, Sugisawa T, Makino H, Abe M, Tsushima M, Yoshimasa Y, Yamashita T, Miyamoto Y, Yamamoto A, Tomoike H, Yokoyama S	Impact of statin treatment on the clinical fate of heterozygous familial hypercholesterolemia.	J Atherosclr Thromb.			2010 In press
Harada-Shiba M, Takamisawa I, Miyata K, Ishii T, Nishiyama N, Itaka K, Kangawa K, Yoshihara F, Asada Y, Hatakeyama K, Nagaya N and Kataoka K	Intratracheal gene transfer of adrenomedullin using polyplex nanomicelles attenuates monocrotaline-induced pulmonary hypertension in rats.	Mol. Ther.	17	1180-1186	2009

Watanabe K, Harada-Shiba M, Suzuki A, Gokuden R, Kurihara R, Sugao Y, Mori T, Katayama Y and Niidome T	In vivo siRNA delivery with dendritic poly(L-lysine) for the treatment of hypercholesterolemia.	Mol. Biosyst.	5	1306-1310	2009
Fujita Y, Kakino A, Harada-Shiba M, Sato Y, Otsui K, Yoshimoto R and Sawamura T	C-reactive protein uptake by macrophage via class A scavenger receptor	Clin. Chem.			2010 In press
Harada K, Miyamoto Y, Morisaki H, Ohta N, Yamanaka I, Kokubo Y, Makino H, Harada-Shiba M, Okayama A, Tomoike H, Okumura T, Saito Y, Yoshimasa Y, Morisaki T	A novel Thr56Met mutation of the autosomal recessive hypercholesterolemia gene associated with hypercholesterolemia.	J. Atheroscler. Thromb.			2010 In press
K. Itaka, K. Osada, K. Morii, P. Kim, S. -H. Yun, K. Kataoka	Polyplex nanomicelle promotes hydrodynamic gene introduction to skeletal muscle.	J. Control. Release			2010 In press

J|A|C|S
ARTICLES

Published on Web 12/10/2009

Chemical Reactions on Surface Molecules Attached to Silicon Quantum Dots

Amane Shiohara,[†] Sanshiro Hanada,[‡] Sujay Prabakar,[†] Kohki Fujioka,[‡] Teck H. Lim,[†] Kenji Yamamoto,[‡] Peter T. Northcote,[†] and Richard D. Tilley*,[†]

School of Chemical and Physical Sciences, MacDiarmid Institute of Advanced Materials and Nanotechnology, Victoria University of Wellington, P.O. Box 600, Wellington, New Zealand, and International Clinical Research Centre, Research Institute, International Medical Centre of Japan, 1-21-1 Toyama, Shinjuku-ku, Tokyo, 162-8655 Japan

Received August 1, 2009; E-mail: richard.tilley@vuw.ac.nz

Abstract: This Article describes research on chemical reactions on molecules attached to the surface of silicon quantum dots that have been performed to produce quantum dots with reactive surface functionalities such as diols and epoxides. Characterization of the surface reactions includes NMR and FT-IR studies, and the quantum dots were characterized by transmission electron microscopy (TEM) and energy dispersive spectroscopy (EDS). Cytotoxicity and cell viability assay conducted on silicon dots capped with polar molecules indicated low toxicity with quantum dots with more reactive functionalities found to be more toxic. The silicon quantum dots photoluminesce and have been used as a blue chromophore for the biological imaging of cells.

Introduction

Quantum dots have several interesting characteristics due to quantum effects that appear at the nanoscale. They have unique optical and electronic properties that are not observed in their bulk counterparts.[1] Because of these characteristics, they have found many applications including in lasers, photosensors, and medical biology.[2−16] Current medical and biological fluorescent imaging is limited to the use of conventional organic dye markers, which have limited photostability. Recently, these have begun to be replaced by quantum dots of materials such as cadmium selenide (CdSe), silicon, and germanium that have several advantages including enhanced photostability.[17−21]

Quantum dots of group II/VI such as CdSe quantum dots are well-known, and substantial research has been conducted on these systems because of their strong luminescence.[21] There have, however, been concerns over the toxicity of these quantum dots in the human body. The toxicity of these quantum dots arises from two main sources: (1) the quantum dot core and (2) the capping molecules.

The cytotoxicity of CdSe quantum dots has been reported by Derfus et al.[22] who illustrated that cell damage could be caused by an uncoated CdSe core under UV excitation. Because of their low toxicity, silicon nanoparticles would be an ideal candidate for biological fluorescence imaging. Silicon has the advantage of being nontoxic and inexpensive, and, over the past few decades, many methods for the synthesis of silicon and germanium quantum dots have been reported. The solution-phase synthesis of silicon quantum dots via a reductive process has been reported by Kauzlarich and co-workers,[23−34] at high

[†] Victoria University of Wellington.
[‡] International Medical Centre of Japan.

(1) Alivisatos, P. A. *J. Phys. Chem.* **1996**, *100*, 13226–13239.
(2) Alivisatos, P. A. *Science* **1996**, *271*, 933.
(3) Bruchez, M., Jr.; Moronne, M.; Gin, P.; Weiss, S.; Alivisatos, P. A. *Science* **1998**, *281*, 2013–2016.
(4) Chan, W. C. W.; Nie, S. *Science* **1998**, *281*, 2016–2018.
(5) Mattousi, H.; Mauro, J. M.; Goldman, E. R.; Anderson, G. P.; Sundar, C. V.; Mikulec, V. F.; Bawendi, G. M. *J. Am. Chem. Soc.* **2000**, *122*, 12142–12150.
(6) Dubertret, B.; Skourides, P.; Norris, D. J.; Noireaux, V.; Brivanlou, A. H.; Libchaber, A. *Science* **2002**, *298*, 1759–1762.
(7) Alivisatos, P. A. *Nat. Biotechnol.* **2004**, *22*, 47–52.
(8) Hoshino, A.; Hanaki, K.; Suzuki, K.; Yamamoto, K. *Biochem. Biophys. Res. Commun.* **2004**, *314*, 46–53.
(9) Hanaki, K.; Momo, A.; Oku, T.; Komoto, A.; Maenosono, S.; Yamaguchi, Y.; Yamamoto, K. *Biochem. Biophys. Res. Commun.* **2003**, *302*, 496–501.
(10) Al-Salim, N.; Young, A. G.; Tilley, R. D.; McQuillan, A. J.; Xia, J. *Chem. Mater.* **2007**, *19*, 5185–5193.
(11) Coe, S.; Woo, W. K.; Bawendi, M. G.; Bulovic, V. *Nature* **2002**, *420*, 800–803.
(12) Santori, C.; Fattal, D.; Vickovic, J.; Solomon, G. S.; Yamamoto, Y. *Nature* **2002**, *419*, 594–597.
(13) Harman, T. C.; Taylor, P. J.; Walsh, M. P.; LaForge, B. E. *Science* **2002**, *297*, 2229–2232.
(14) Li, X.; Wu, Y.; Steel, D.; Gammon, D.; Stievater, T. H.; Katzer, D. S.; Park, D.; Piermarocchi, C.; Sham, L. J. *Science* **2003**, *301*, 809–811.
(15) Beham, E.; Stufler, S.; Findeis, F.; Bichler, M.; Abstreiter, G.; Zrenner, A. *Nature* **2002**, *418*, 612–614.
(16) Xu, S.; Kumar, S.; Nann, T. *J. Am. Chem. Soc.* **2006**, *128*, 1054–1055.
(17) Che, J.; Wang, X.; Xiao, Y.; Wu, X.; Zhou, L.; Yuan, W. *Nanotechnology* **2007**, *18*, 135706.
(18) Alsharif, N. H.; Berger, C. E. M.; Varanasi, S. S.; Chao, Y.; Horrocks, B. R.; Datta, H. K. *Small* **2009**, *5*, 221–228.
(19) Zou, J.; Kauzlarich, S. M. *J. Cluster Sci.* **2008**, *19*, 341–355.
(20) Warner, J. H.; Tilley, R. D. *Nanotechnology* **2006**, *17*, 3745–3749.
(21) Nirmal, M.; Dabbousi, B. O.; Bawendi, M. G.; Macklin, J. J.; Trautman, J. K.; Harris, T. D.; Brus, L. E. *Nanotechnology* **1996**, *383*, 802–804.
(22) Derfus, A. M.; Chan, W. C. W.; Bhatia, S. N. *Nano Lett.* **2004**, *4*, 11–18.
(23) Neiner, D.; Chiu, H. W.; Kauzlarich, S. M. *J. Am. Chem. Soc.* **2006**, *128*, 11016–11017.
(24) Baldwin, R. K.; Zou, J.; Pettigrew, K. A.; Yeagle, G. J.; Britt, R. D.; Kauzlarich, S. M. *Chem. Commun.* **2006**, *6*, 658–660.

10.1021/ja906501v

temperatures and pressures by Korgel and co-workers,[35−40] and microemulsion synthesis.[41,42]

The surface modification of silicon quantum dots is very important to impart functionalities. Because silicon quantum dots are able to be covalently bound to carbon- or oxygen-containing molecules, there are a few reports on silicon quantum dots capped with hydrophobic molecules such as 1-heptene.[43] The preparation of water-dispersible silicon quantum dots that maintain their photoluminescence stability has been proved to be difficult. Acrylic acid (PAAc) coated silicon quantum dots have been reported by Ruckenstein et al.[44] These silicon quantum dots were stable in aqueous solutions with good photoluminescent stability. Swihart et al.[45] also reported propionic acid coated silicon quantum dots. In both cases, silicon quantum dots were capped under UV light irradiation. We have reported the synthesis of amino-terminated silicon quantum dots made in reverse micelle system and capped with allylamine using a platinum catalyst.[46] However, reports describing the surface modification of silicon quantum dots are still few. Additionally, most of the surface capping protocols are single step processes in which the target molecules are directly attached onto the surface. In this study, our technique of surface modification is multistepped based on the chemistry of the terminal double bond on the surface to achieve the target functionalities. The reason for adopting a stepwise approach is that when attaching functional molecules to the surface of silicon quantum dots some of the molecules tend to have more than one reactive moiety. For example, molecules with an oxygen containing functional group such as carboxylic group or hydroxy group and a double bond may preferentially react with the oxygen functionality, not the carbon double bond. The approach we have adopted enables the formation of silicon quntum dots functionalized with a broad range of functional groups including highly reactive species such as epoxides.

Different surface modifications can induce different levels of quantum dot toxicity. Thus, a detailed examination of the toxicity of quantum dots with various capping molecules is essential for the widespread understanding of the application of quantum dots in biological imaging.

In this study, silicon quantum dots were synthesized by microemulsion synthesis. Silicon quantum dots were characterized by transmission electron microscopy (TEM) and energy dispersive spectrometry (EDS). Quantum dots were purified by liquid-phase separation and column chromatography. We also introduce methods for producing silicon quantum dots with different surface modifications with a view toward biomedical applications. The capping of the silicon quantum dots has been fully characterized using nuclear magnetic resonance (NMR) and Fourier transform infrared spectroscopy (FTIR). The cytotoxicity of quantum dots with different surface modifications has been evaluated, and the optimal surface capping in terms of lowest toxicity has been established.

Experimental Section

Synthesis of Surface Passivated Silicon Quantum Dots. All reactions were performed in a nitrogen filled glovebox. In a typical experiment, 0.002 mol of $SiBr_4$ (0.3 mL) was dissolved using a homogenizer in either 1.5 g of TOAB and 100 mL of anhydrous toluene or 1.5 g of $C_{12}E_5$ and 100 mL of anhydrous hexane. Hydrogen-terminated silicon nanoparticles were formed by adding a stoichiometric amount of reducing agent. Hydrophobic and hydrophilic particles were formed by modifying the surface silicon−hydrogen bonds by reaction with 92 μL of 0.1 mol H_2PtCl_6 in isopropanol as catalyst and 4 mL of either allylamine or 1,5-hexadiene.

Purification of Silicon Quantum Dots. Liquid-phase separation was applied to alkene-terminated silicon quantum dots. All of the solvent was removed under vacuum, and 100 mL of hexane was added followed by 5 min sonication. The solution was transferred to a separation funnel and washed with *N*-methylformamide (Aldrich) three times. The organic layer was extracted and washed with water three times. The organic layer was then concentrated to give alkene-terminated silicon quantum dots.

Amine-terminated silicon quantum dots were purified by size exclusion column chromatography. The solvent was removed under vacuum, and 50 mL of methanol was added to dissolve the particles. The solution was sonicated for 5 min and filtered through a Millipore 0.45 μm filter paper. The filtrate was concentrated down to 1 mL and was put into the column (ϕ = 1 cm, 41.0 cm). Sephadex gel LH-20 (beads size 25−100 μm) was used as the stationary phase. Flow rate was a drop per 5 s, and fractions were collected every 50 drops. Each fraction was checked for luminescence under a UV lamp (365 nm). The luminescent fraction was collected and concentrated down to 1 mL to give pure amine-terminated silicon quantum dots.

Chemical Reactions on the Surface of Silicon Quantum Dots. a. Epoxide-Terminated Silicon Quantum Dots. Epoxide-terminated silicon quantum dots were synthesized from alkene-terminated silicon quantum dots. 0.4 g (1.5 equiv) of chloroperoxy benzoic acid (*m*-CPBA: Aldrich) was added to a solution of alkene-terminated silicon quantum dots in 20 mL of CH_2Cl_2. The reaction mixture was stirred for 6 h and quenched with a saturated solution of Na_2SO_3. The aqueous phase was extracted with CH_2Cl_2, and the combined organic solution was washed with 10% NaOH solution. The organic layer was collected, and $MgSO_4$ was added to absorb water. The solution was filtered and concentrated under reduced pressure to give epoxide-terminated silicon quantum dots.

(25) Zou, J.; Baldwin, R. K.; Pettigrew, K. A.; Kauzlarich, S. M. *Nano Lett.* **2004**, *4*, 1181–1186.
(26) Tanke, R. S.; Kauzlarich, S. M.; Patten, T. E.; Pettigrew, K. A.; Murphy, D. L.; Thompson, M. E.; Lee, H. W. H. *Chem. Mater.* **2003**, *15*, 1682–1689.
(27) Liu, Q.; Kauzlarich, S. M. *Mater. Sci. Eng., B* **2002**, *96*, 72–75.
(28) Baldwin, R. K.; Pettigrew, K. A.; Ratai, E.; Augustine, M. P.; Kauzlarich, S. M. *Chem. Commun.* **2002**, *17*, 1822–1823.
(29) Baldwin, R. K.; Pettigrew, K. A.; Garno, J. C.; Power, P. P.; Liu, G. Y.; Kauzlarich, S. M. *J. Am. Chem. Soc.* **2002**, *124*, 1150–1151.
(30) Mayeri, D.; Phillips, B. L.; Augustine, M. P.; Kauzlarich, S. M. *Chem. Mater.* **2001**, *13*, 765–770.
(31) Yang, C. S.; Bley, R. A.; Kauzlarich, S. M.; Lee, H. W. H.; Delgado, G. R. *J. Am. Chem. Soc.* **1999**, *121*, 5191–5195.
(32) Zhang, X.; Brynda, M.; Britt, R. D.; Carroll, E. C.; Larsen, D. S.; Louie, A. Y.; Kauzlarich, S. M. *J. Am. Chem. Soc.* **2007**, *129*, 10668–10669.
(33) Zhang, X.; Neiner, D.; Wang, S.; Louie, A. Y.; Kauzlarich, S. M. *Nanotechnology* **2007**, *18*, 9–095601.
(34) Zou, J.; Sanelle, P.; Pettigrew, K. A.; Kauzlarich, S. M. *J. Cluster Sci.* **2006**, *17*, 565–578.
(35) Lu, X. M.; Korgel, B. A.; Johnston, K. P. *Nanotechnology* **2005**, *16*, S389.
(36) Lee, D. C.; Hanrath, T.; Korgel, B. A. *Angew. Chem., Int. Ed.* **2005**, *44*, 3573–3577.
(37) Pell, L. E.; Schricker, A. D.; Mikulec, F. V.; Korgel, B. A. *Langmuir* **2004**, *20*, 6546–6548.
(38) Hanrath, T.; Korgel, B. A. *Adv. Mater.* **2003**, *15*, 437–440.
(39) English, D. S.; Pell, L. E.; Yu, Z. H.; Barbara, P. F.; Korgel, B. A. *Nano Lett.* **2002**, *2*, 681–685.
(40) Holmes, J. D.; Ziegler, K. J.; Doty, R. C.; Pell, L. E.; Johnston, K. P.; Korgel, B. A. *J. Am. Chem. Soc.* **2001**, *123*, 3743–3748.
(41) Tilley, R. D.; Yamamoto, K. *Adv. Mater.* **2006**, *18*, 2053–2056.
(42) Wilcoxon, J. P.; Samara, G. A.; Provencio, P. N. *Phys. Rev. B* **1999**, *60*, 2704–2714.
(43) Tilley, R. D.; Warner, J. H.; Yamamoto, K.; Matsui, I.; Fujimori, H. *Chem. Commun.* **2005**, *14*, 1833–1835.
(44) Li, Z. F.; Ruckenstein, E. *Nano Lett.* **2004**, *4*, 1463–1467.
(45) Sato, S.; Swihart, M. T. *Chem. Mater.* **2006**, *18*, 4083–4088.
(46) Warner, J. H.; Hoshino, A.; Yamamoto, K.; Tilley, R. D. *Angew. Chem., Int. Ed.* **2005**, *44*, 4550–4554.

Scheme 1. Reactions on Surface Molecules Bound to Silicon Quantum Dots

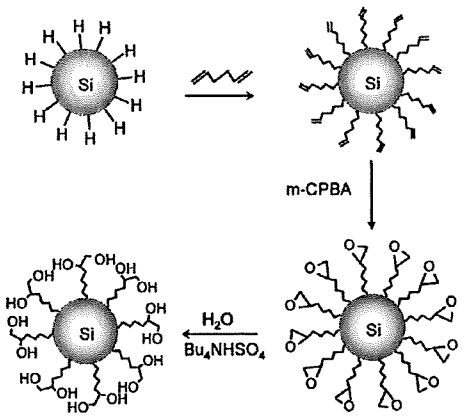

b. Diol-Terminated Silicon Quantum Dots. 8.5 mg (0.025 mmol) of phase transfer catalyst, tetrabuthylammonium hydrogen sulfate (Bu_4NHSO_4), in H_2O (2.0 mL) was added to a solution of epoxide-terminated silicon quantum dots in $CHCl_3$. The mixture solution was stirred for 24 h at 45 °C. The mixture was extracted with diethyl ether (3 × 10 mL), and the combined organic layer was dried over Na_2SO_4. The solution was concentrated under reduced pressure to give diol-terminated silicon dots.

FTIR Spectroscopy. A Perkin-Elmer FT-IR spectrometer was used to identify and characterize the structure of the molecules attached to the nanoparticle surfaces. A KBr pellet was prepared by grinding powder KBr and a drop of each silicon quantum dot solution.

^{1}H NMR Spectroscopy. ^{1}H NMR (500 MHz) spectra of samples in $CDCl_3$ were recorded on a Varian Unity Inova 500 MHz spectrometer. The solvent of each sample solution was removed by evaporation using a rotary evaporator at 60 °C. After removal of the solvent, the sample was freeze-dried overnight and dissolved in $CDCl_3$.

Cytotoxicity Evaluation. For the cytotoxicity assays, WS1, A549, and HepG2 cells were used. WS1 and A549 were tested for epoxide- and diol-terminated silicon quantum dots, and HepG2 was used for amine-terminated silicon quantum dots.

We inoculated 10 000 cells in each well of 96-well plates and cultured them for 48 h at 37 °C/5% CO_2. Next, each type of silicon quantum dots was added in the indicated concentrations and cocultured for 48 h for WS1 and A549 cells and 1 h for HepG2 cells. The cytotoxicities of these quantum dots were examined in a cell viability assay. We used a Cell Counting Kit-8 (Dojindo, Japan) to measure the succinate dehydrogenase mitochondrial activity. The 450 nm absorption of formazans produced by the enzyme was measured with a DTX 880 (Beckman Coulter, Inc., USA) microplate reader ($n = 3$). The activities were calculated as the ratio of the absorbance value against those of the control.

Cell Imaging. Silicon quantum dots capped with allylamine were applied for cell imaging. HepG2 cells were used. The assay was conducted at 1.0 μg/mL for 6 h incubation. The image was taken on a fluorescent microscope IX-81 (Olympus) with an excitation filter 330−380 nm.

Results and Discussion

Silicon quantum dots were synthesized by a microemulsion route. Silicon tetrabromide was used as the silicon precursor and reduced by strong hydride reducing agents. Hydrogen-terminated silicon quantum dots produced were capped with organic molecules by using a Pt-based catalyst or exposure to UV radiation.

The surface modification reactions performed are shown in Scheme 1. Alkene-terminated silicon quantum dots were synthesized by capping with 1,5-hexadiene. The direct reaction of hydride-terminated silicon quantum dots with alkenes containing alcohol and epoxide functional groups leads to complex reactions between the quantum dots and the oxygen functional group. Thus, epoxy-terminated and diol-terminated silicon quantum dots were synthesized by direct reaction of diene functional groups on the surface of the silicon quantum dots. Silicon quantum dots were reacted with allylamine to produce silicon quantum dots with amine functional groups on their surface.

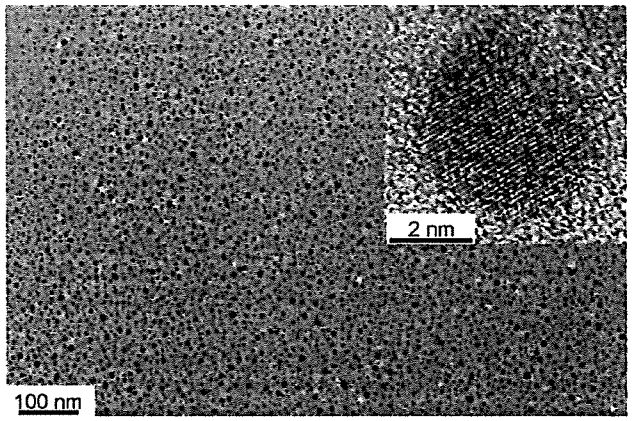

Figure 1. TEM image of amine-terminated silicon quantum dots and inset showing a high-resolution TEM image of an individual silicon nanocrystal.

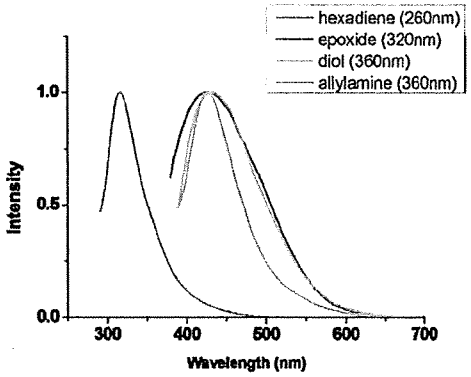

Figure 2. Photoluminescence spectra of silicon quantum dots capped with hexadiene-, epoxide-, diol-, and amine-terminated silicon quantum dots. *Y* axis shows normalized intensity.

Electron Microscopy. Figure 1 shows the TEM images of silicon quantum dots capped with allylamine. The amine capped silicon quantum dots produced ranged in size from 1.5 to 10 nm. The amine capped nanoparticles have an average diameter of 3.7 ± 0.9 nm, which is close to the exciton Bohr radius of silicon (4.3 nm). TEM images of the diene and diol samples are shown in Figures S-1 and S-2 (see the Supporting Information) and were similar in size to the amine capped silicon quantum dots having average sizes of 3.6 and 3.4 nm, respectively. From the TEM images, the particle sizes were relatively monodisperse, and aggregation of the nanoparticles was not observed. EDS analysis of the sample further confirmed the presence of silicon.

Optical Properties. Figure 2 shows the photoluminescence (PL) spectra of silicon quantum dots terminated with hexadiene, epoxy, diol, and amine functional groups. The nanoparticles were excited at 260 nm (hexadiene capped), 320 nm (epoxide-

terminated), and 360 nm (diol- and amine-terminated). The emission peak position of the silicon quantum dots capped with nonpolar hexadiene is around 320 nm. In comparison, the emission peak of silicon quantum dots capped with the polar functionalities, epoxide, diol, and allylamine, is around 430 nm. Full photoluminescence (PL) spectra of silicon quantum dots capped with hexadiene-, epoxy-, diol-, and amine-terminated silicon quantum dots over a range of excitation wavelengths are shown in Figure S-3 (see the Supporting Information). The absorption spectra of the silicon quantum dots with different surface terminations are shown in Figure S-4 (see the Supporting Information).

The origin of the photoluminescence in silicon quantum dots is complicated by the presence of both indirect and direct band gap transitions. The blue luminescence shown in Figure 2 has been previously observed for silicon quantum dots and can be attributed to the $\Gamma-\Gamma$ direct band gap transition and is in good agreement with previous reports.[40,42,46,47]

The observation that silicon quantum dots capped with nonpolar diene have a higher energy emission than the quantum dots terminated with polar epoxy, diol, and amine functional groups is of interest and similar to previous observations comparing the optical properties of silicon quantum dots capped with nonpolar and polar molecules.[47] From the TEM images of these samples, shown in Figures 1, S-1, and S-2 (see the Supporting Information), it can be seen that the nanocrystal sizes are almost identical, and therefore the origin of the difference in the energy of the emission is most likely due to the nature of the surface capping and environment.[47] This result provides direct evidence that the surface-capping molecule plays an important role in the radiative recombination mechanisms in 2−4 nm silicon nanocrystals. The difference in the emission is most likely due to different radiative recombination pathways for polar and nonpolar capped silicon nanocrystals.[47] Theoretical studies have shown that it is possible for the electronic charge distribution of polar-capped silicon nanocrystals to be modified by the polar nature of cappings ligand, leading to the band gap being slightly lower for polar capped silicon nanocrystals than for nonpolar capped silicon nanocrystals, and this may be occurring in our samples.[48−50]

FTIR Studies. To confirm the surface modification is successful, the nanoparticles were further characterized by FTIR and NMR. Figure 3 shows the FTIR spectra of alkene-, epoxy-, and diol-terminated silicon quantum dots, respectively.

For the hexadiene capped silicon quantum dots spectrum, Figure 3d, two peaks observed at 1460 and 1260 cm^{-1} are attributed to the vibrational scissoring and symmetric bending of $Si-CH_2$, respectively, and these peaks can be seen in all three spectra. This clearly indicates that one of the double bonds of hexadiene has reacted with the silicon−hydrogen bond on the surface of the quantum dots to for a silicon carbon bond. The peak at 1640 cm^{-1} of alkene-terminated silicon dot corresponds to the CH_2=CH stretch vibration of the terminated double bond. This peak cannot be seen in the other two spectra.

In the spectrum of epoxy-terminated silicon quantum dots, Figure 3c, the peak of epoxy ring symmetrical stretching can be observed at 1217 cm^{-1}. The peak at 1640 cm^{-1} corresponding

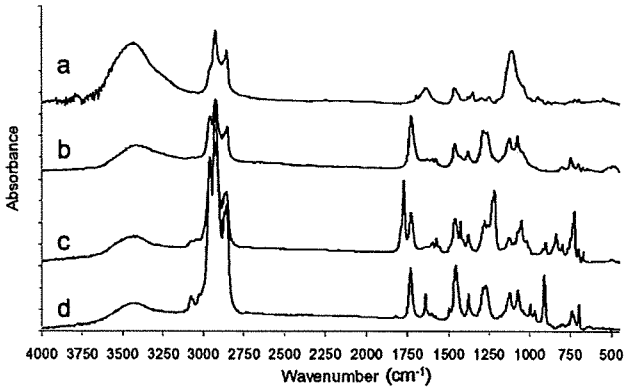

Figure 3. FTIR spectra of silicon quantum dots capped with (a) amine, (b) diol, (c) epoxy, and (d) diene.

to the CH_2=CH terminated double bond has also disappeared, implying oxidation of the terminal double bond to the epoxide.

In Figure 3b, evidence for the hydrolytic ring-opening from the epoxy group to a diol is shown by the peak corresponding to an O−H vibration of an alcohol group as can be seen at 1285 cm^{-1} and the disappearance of the epoxide ring stretch.

For allylamine capped silicon quantum dots, Figure 3a, peaks observed at 1460 and 1248 cm^{-1} are attributed to $Si-CH_2$ vibrational scissoring and symmetric bending. The absorbance from 3500 to 3655 cm^{-1} is attributed to the N−H stretch of an amine. The peak at 1630 cm^{-1} is attributed to allylamine N−H scissoring. The peaks around 2850 and 2925 cm^{-1} represent alkane C−H stretching.

NMR Studies. The surface state of silicon quantum dots was also confirmed by NMR. Figure 4 shows the NMR spectra of each type of silicon quantum dot.

The peaks in Figure 4d, corresponding to the alkene-terminated quantum dots, at δ 4.85 (doublet, 9.0 Hz), δ 4.92 (doublet, 16.9 Hz), and δ 5.72 (multiplet) are typical of a terminal alkene and indicate the formation of silicon quantum dots with a free terminated alkene bond.

The peaks of the terminal alkene are absent in the spectrum of epoxy-terminated silicon quantum dots, Figure 4c, and are replaced by peaks at 2.39, 2.67, and 2.82 ppm, which indicate the presence of an epoxy ring and are similar to the peaks seen in free 1-epoxyhexane.

Upon hydrolysis of the epoxide to the diol, these peaks shift to slightly higher ppm, to 3.36−3.67 ppm consistent with the epoxide ring being opened, shown in Figure 4b.

The allylamine coated silicon quantum dots, Figure 4a, have a quartet peak between 3.70 to 3.75 ppm. This peak is attributed to the protons next to amine group. Also, the protons of the amine group were observed in the peak at 1.25 ppm. All of the NMR data were taken after removal of all volatile starting materials under vacuum at 60 °C. The boiling points of 1,5-hexadiene and allylamine are 60 and 53 °C, respectively; therefore, the peaks observed in the spectra were not from free capping molecules, which all have low boiling points, but from the surface moieties on the silicon quantum dots.

Cytotoxicity Evaluation. Cell viability assay (MTT assay) was applied for cytotoxicity evaluation. Human skin fibroblasts (WS1) and lung epithelial cells (A549) were used for epoxide-terminated and diol-terminated silicon quantum dot because the skin and lungs have higher possibilities of exposure through different mechanisms. The results of the cell viability assay are shown in Figure 5. As can be seen in the figure, epoxide-

(47) Warner, J. H.; Rubinsztein-Dunlop, H.; Tilley, R. D. *J. Phys. Chem. B* **2005**, *109*, 19064–19067.
(48) Reboredo, F. A.; Galli, G. *J. Phys. Chem. B* **2005**, *109*, 1072.
(49) Walker, B. G.; Hendy, S. C.; Gebauer, R.; Tilley, R. D. *Eur. Phys. J. B* **2008**, *66*, 7–15.
(50) Zhou, Z.; Brus, L.; Friesner, R. *Nano Lett.* **2003**, *3*, 163.

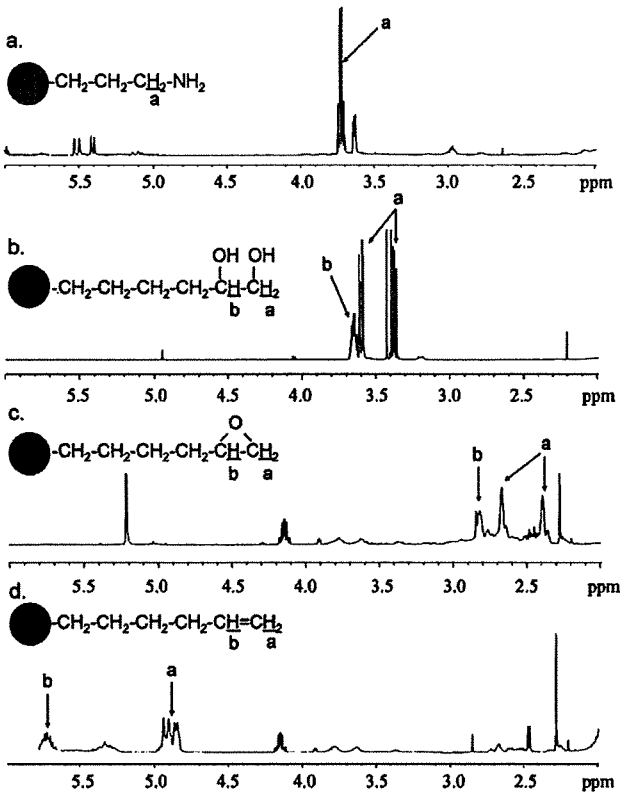

Figure 4. ^{1}H NMR spectra of silicon quantum dots capped with (a) amine, (b) diol, (c) epoxy, and (d) diene (500 MHz, $CDCl_3$).

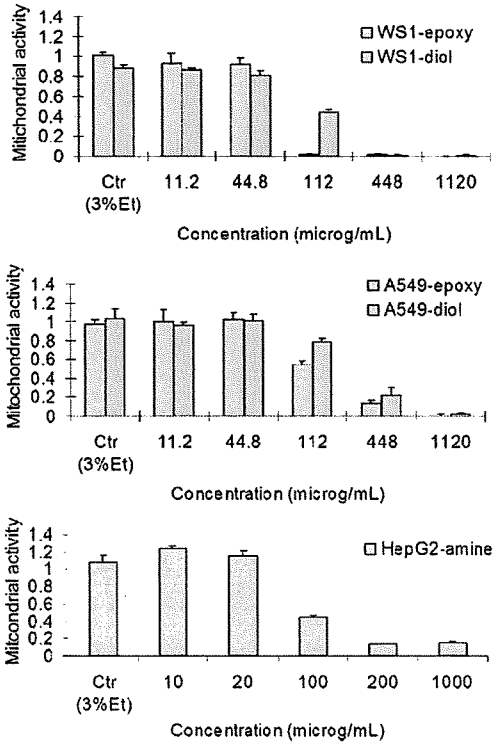

Figure 5. MTT assay of silicon quantum dots. A549 and WS1 with epoxyhexane and hexandiol capped silicon quantum dots and HepG2 with amine capped silicon quantum dots.

terminated quantum dot cytotoxicity appears at a concentration of 112 μg/mL. In comparison, the diol-terminated silicon

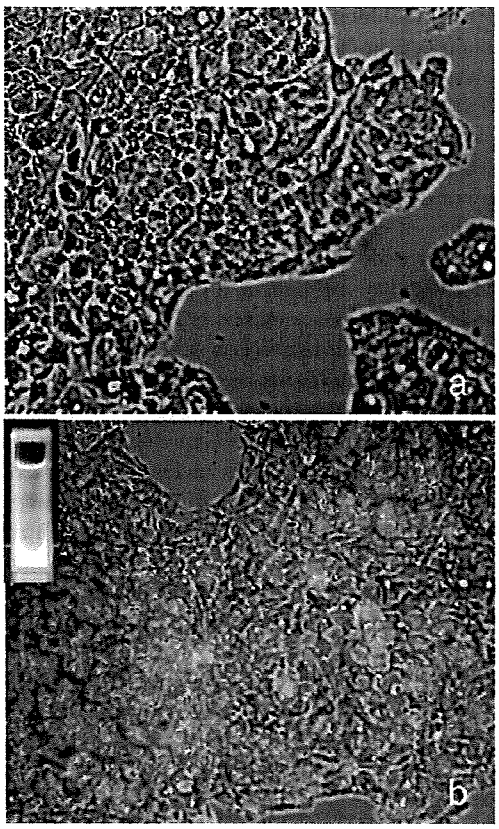

Figure 6. Cell imaging using silicon quantum dots capped with allylamine. (a) Transmitted light image and fluorenscent image of negative control; (b) transmitted light image and fluorescent image of silicon quantum dots at 1.0 μg/mL, respectively.

quantum dots did not show toxicity at this level but at 448 μg/mL. The epoxide group is a highly reactive species and known to have oxidative toxicity, and so it is in agreement with expectations that it has a higher toxicity than the diol.[51] The 50% inhibition coefficients of epoxide-terminated silicon quantum dots for WS1 cell and A549 cell were 0.068 and 0.13 mg/mL, respectively. In comparison, cytotoxicity for the diol-terminated silicon quantum dots did not appear up to 0.097 and 0.225 mg/mL for WS1 cell and A549 cell lines, which is almost double the concentration as compared to epoxide-terminated quantum dots. These figures are comparable to previous studies on quantum dots that have relatively low toxicity.[52–54] The reason why the 50% inhibition coefficients of both sets of silicon quantum dots were higher for A549 than WS1 cell lines is most likely due to the difference of the metabolism of each cell line, which would affect the uptake of the silicon quantum dots.

To compare the toxicity beyond these two cell lines, toxicity on liver cell was evaluated with amine-terminated silicon quantum dots. The liver has the function to reduce toxicity by albumin secretion or glucuronate conjugation among the tissues in which quantum dots may accumulate. The results showed

(51) Hemminki, A.; Väyrynen, T.; Hemminki, K. *Chem.-Biol Interact.* **1994**, *93*, 51–58.
(52) Chang, E.; Thekkek, N.; Yu, W. W.; Colvin, V. L.; Drezek, R. *Small* **2006**, *2*, 1412–1417.
(53) Manzoori, K.; Johny, S.; Thomas, D.; Setua, S.; Menon, D.; Nair, S. *Nanotechnology* **2009**, *20*, 065102.
(54) Fujioka, K.; Hiruoka, M.; Sato, K.; Manabe, N.; Miyasaka, R.; Hanada, S.; Hoshino, A.; Tilley, R. D.; Manome, Y.; Hirakuri, K.; Yamamoto, K. *Nanotechnology* **2008**, *19*, 415102.

that the 50% inhibition coefficient of amine-terminated silicon quantum dots in the hepatoma cell line (HepG2) was 0.1 mg/mL, which is similar to the diol-terminated silicon quantum dots in WS1 cells. The results imply safe uses of silicon quantum dots in biological application below these concentration thresholds.

Cell Imaging. Figure 6 shows the cell imaging of silicon quantum dots capped with allylamine. This image shows the suitability of allylamine-capped silicon quantum dots as a chromophore for biological imaging. For the images in Figure 6, an excitation wavelength of 365 nm was used, and the emission at 480 nm was monitored. The control image (Figure 6a) shows minimal fluorescence from the HeLa cells relative to the HeLa cells with the incorporated silicon quantum dots (Figure 6b). Thus, the fluorescence observed in the HeLa cells in Figure 6b arises from the emission from silicon quantum dots. The inset in the top left corner of Figure 6b shows the bright blue fluorescence from a vial of allylamine capped silicon quantum dots in water when excited with UV light. The bright blue fluorescence from the silicon quantum dots is distributed uniformly and shows that the silicon quantum dots were taken up into the cytoplasm. This result shows the possibility of using these hydrophilic silicon quantum dots as chromophores in biological fluorescence imaging.

Conclusions

Chemical reactions on the molecules attached to the surface of silicon quantum dots have been performed to produce quantum dots with reactive surface functionalities such as diols and epoxides. These quantum dots are relatively monodisperse and exhibit luminescence under UV excitation. The results from cytotoxicity studies indicate that toxicity is dependent on the surface functionality and that the silicon quantum dots as prepared have potential in biological applications such as bioimaging. This research opens the door for future biological applications of silicon quantum dots.

Acknowledgment. R.D.T. thanks the MacDiarmid Institute for funding. A.S., S.P., T.H.L., and R.D.T. thank FRST for funding through Grant IIOF VICX0601.

Supporting Information Available: TEM images and optical properties. This material is available free of charge via the Internet at http://pubs.acs.org.

JA906501V